Validating molecular dynamics with direct imaging of radiation damage debris

P. D. Lane,[1] G. J. Galloway,[1] R. J. Cole,[1] M. Caffio,[2] R. Schaub,[2] and G. J. Ackland[1]
[1]*School of Physics, SUPA and CSEC, The University of Edinburgh, Edinburgh EH9 3JZ, Scotland, United Kingdom*
[2]*EaStCHEM School of Chemistry, University of St. Andrews, KY16 9ST, Scotland, United Kingdom*
(Received 7 February 2012; published 29 March 2012)

We present a combined experimental and simulation approach to studying the primary damage caused by ion irradiation. We have examined a surface of copper subjected to 500 eV Ar^+ ion bombardment using scanning tunnelling microscopy (STM) and observed craterlike regions of damage, with a central hole surrounded by adatoms. Molecular dynamics (MD) simulations reproduce this structure and enable us to study the formation process. We find both qualitative and quantitative agreement between the defect structures observed in STM and MD, providing a rare direct validation of the MD simulation. We observe a process in which a stress wave produces defect clusters fully formed at the surface, in contrast to the conventional bulk picture of creation, migration, and aggregation of point defects. This produces a characteristic crater structure. We also observe one-dimensional stress propagation events, which produce defects far from the initial collision and cooling of the thermal spike without self diffusion.

DOI: 10.1103/PhysRevB.85.094111 PACS number(s): 68.37.Ef, 02.70.Ns, 61.80.Jh, 61.82.Bg

I. INTRODUCTION

Damage to metals by irradiation is a key process which can determine the safe operating lifetime of nuclear reactors and spacecraft. When high-energy particles strike a material, a *cascade* of damage occurs which results ultimately in the formation of vacancy and interstitial defects. Such events occur rapidly in the bulk of the material and are impossible to study directly. Most of our knowledge of this process comes from computer simulation which shows that cascades produce primary damage in the form of vacancies, interstitials, and small clusters of these defects. In time, the clusters aggregate to form larger defects such as voids and dislocation loops which can be imaged using transmission electron microscopy (TEM) on thin samples.

The amount of radiation damage is typically measured by displacements per atom (DPA). Experimentally, this is a self-consistent quantity which enables good comparison between bombardment with different ions and at different energies. However, the numerical definition of DPA[1] in terms of the number of primary defect Frenkel pairs produced by binary collision approximation (BCA) calculations[2] has consistently been found to be at variance with molecular dynamics (MD) calculation by a factor of three. This becomes especially important when the yield of primary damage is fed as an input into higher level simulations, such as kinetic Monte Carlo. Moreover, it provides some estimate of the safe lifetime of reactors: the lifetime extensions now being implemented worldwide are made possible by the historical overestimation of the amount of damage. However, the lack of experimental validation of these calculations means that they continue to be treated with scepticism by licensing and regulatory bodies, potentially neglecting a valuable source of safety-related information.

Although it is generally accepted that the MD approach[3–7,10–19] is more reliable than the BCA, neither are backed by direct experimental data which count the defects at the atomic level.

Experiments have concentrated on observing microstructures such as dislocation loops and voids and, in Cu and other fcc materials, vacancies stacking fault tetrahedra which impede dislocation motion leading to hardening.[17,20] Recent low-dose irradiation of Mo single-crystal foils revealed the formation of vacancy loops from a single cascade collapse,[21] in contrast to the situation in Fe.[22] In Ni and Cu, nanostructuring[11,23,24] has been predicted by MD and shown experimentally, to improve radiation resistance, while the movement of multidefect structures such as dislocation loops remains system dependent.[25–28] There has even been comparison with cosmic-ray erosion[29] and crater removal.[10]

Crater structure and its energy dependence have been studied using Lennard Jones potentials,[30] which show excellent qualitative agreement with the experiment for the power-law relation in variation of crater size with impact energy. However, the quantitative yields disagree by typically a factor of five, probably due to the unphysically high formation energy for point defects in Lennard Jonesium.

In this paper, we demonstrate a method which enables us to observe primary yield damage experimentally at the atomic level and compare it with analogous molecular dynamics simulations. These findings give a direct experimental validation of the methodology behind a huge body of existing simulational work.

Our approach is to irradiate highly polished Cu samples with low-dose 500 eV ions causing damage cascades close to the surface. Individual defects which are created at, or migrate to, the surface are then observed at subnanometer resolution using scanning tunnelling microscopy (STM). Exactly the same system is then examined using molecular dynamics simulation.

II. EXPERIMENTAL PROCEDURE

The experiments were performed in an ultrahigh-vacuum chamber with a base pressure below 10^{-10} mbar and at a temperature of 144 K, obtained by liquid-nitrogen cooling of the sample manipulator. The sample was a high quality Cu single-crystal aligned within 0.1° of (110), less than one step plane per 100 atoms. It was prepared using multiple cycles of Ar^+ ion bombardment (30° incidence, 500 eV, 0.25 $\mu A/cm^2$, 15 min, 300 K) and subsequent annealing to 840 K. Surface cleanliness was confirmed by a sharp

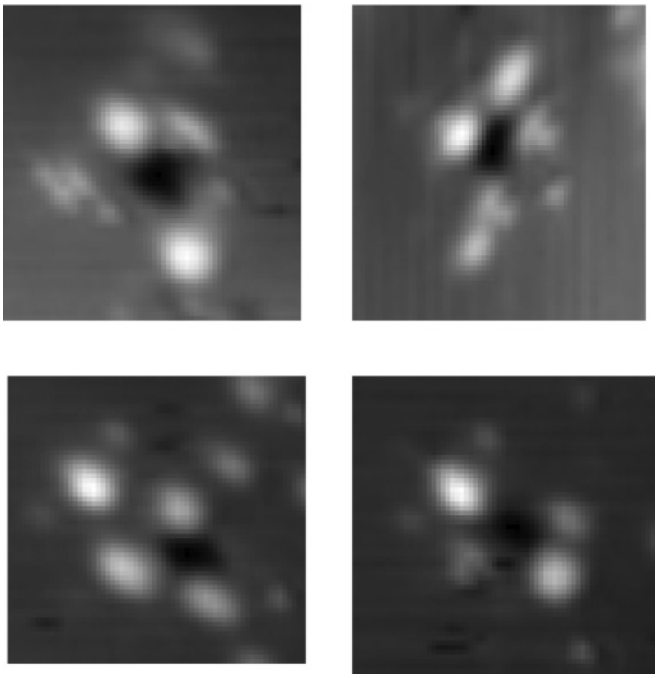

FIG. 1. STM images of craters above cascades; all images are 4×4 nm. The vacancies (dark) lie in the center of the crater and the interstitials form a surrounding halo. The number of vacancies/adatoms are calculated by dividing the total area occupied by vacancies/adatoms on the surface by the area of the unit cell.

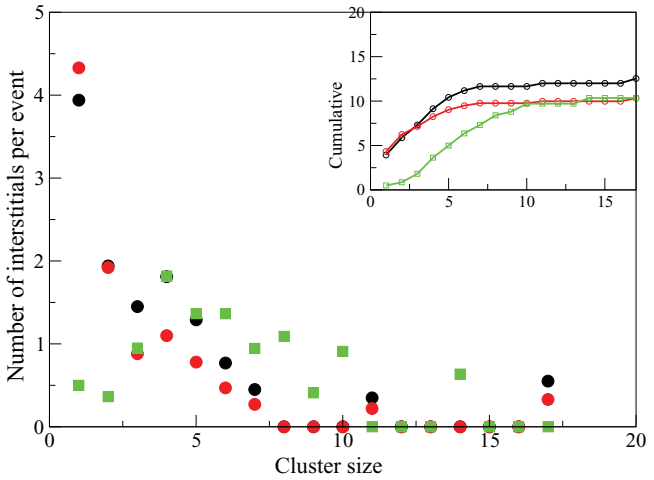

FIG. 2. (Color online) Frequency distribution of interstitial cluster sizes for the experimental (green squares) and theoretical (red circles, all data; black circles, all collisions causing at least three Frenkel pairs). Main graph: mean number of adatoms per impact in clusters of a given size. Inset: cumulative number of adatoms.

(1×1) low-energy electron diffraction pattern and a reflection anisotropy spectroscopy[31] signal indicative of a clean ordered surface.[32,33] STM measurements were performed with *W* tips, in constant current mode with a tunnelling current in the 0.5–1.0 nA range. STM measurements were recorded within 30–90 min after Ar^+ bombardment (0° incidence, 500 eV, 2 s, 144 K, equivalent to 0.0028 ions per unit cell). Multiple images recorded in this time suggest that the craters are immobile. Under these conditions we expect ballistic collision directly between ions, with cascades initiated by collisions between the incoming Ar and Cu atoms.

Representative STM images obtained for the irradiated sample are shown in Fig. 1. It appears that more interstitial defects (white) arrive at the surface than vacancies (dark), with vacancies clustered in a single central void. The topographic appearance of clusters and voids is influenced by STM-tip convolution. To account for this, we estimate the cluster size by calculating the surface area within 2 Å of the observed edge (assuming our STM tip to be typically of 2Å radius) and dividing by the area of an atom.

A set of 30 images was studied to determine statistics (Fig. 2). The adatom cluster size distribution peaked at 4–5 atoms with an average 10.4 ± 6 adatoms per event. By contrast 9.2 ± 3 vacancies are accounted for by the central crater area. These results are qualitatively similar to previous work on silver (001).[34]

III. COMPUTATIONAL DETAILS

To investigate further we applied molecular dynamics using the MOLDY code[35] with 250 000 atom cells, which proved sufficient to contain the cascade. Copper was described using a Finnis-Sinclair potential well tested on surfaces and cascades,[36–38] which breaks the energy into a pairwise core/screened Coulomb repulsion and a second moment tight-binding term describing the valence electrons. Argon has the same electronic core and in a copper environment will have the same screening, so we used the same pairwise potential to describe Ar-Cu interactions, with the appropriate adjustment for ionic charge in the short-range Biersack-Ziegler function.[39] There is no binding term for Ar because it has no valence electrons. Electronic stopping is accounted for by the use of a thermostat, but at the energies used in the experiment nuclear stopping is the dominant effect and the Biersack-Ziegler is the standard way to treat this.

Matching the experiment, the MD used periodic boundary conditions in the (001) and $(\bar{1}10)$ directions and free surface in (110), $(180 \times 128 \times 128$ Å). The simulations began with 500 eV argon atoms 3.5 Å above the surface moving with an angle within 5° of the normal. We used the canonical (NVT) ensemble at 144 K, with the Nose-Hoover parameter set to match the macroscopic thermal conductivity.[40] The Nose-Hoover algorithm also produces a drag force on the incoming ion, which is the simplest model for loss to electronic excitations.[41,42]

The MD system was thermalized for 10 ps, after which the ion was introduced. Verlet integration with variable time stepping was used, scaled with the largest single-atom kinetic energy: a 0.2 fs time step was the smallest required, increasing to 1 fs. No systematic violation of energy conservation was observed.

For analysis the final distribution of atomic positions was mapped onto a reference set from the initial positions. Adatoms and vacancies are identified with empty sites below the reference surface or occupied sites above. An interstitial was defined as having two atoms within 0.5 lattice spacings of a reference site, unless an adjacent vacancy was identified; although never seen at 144 K, this latter condition due to

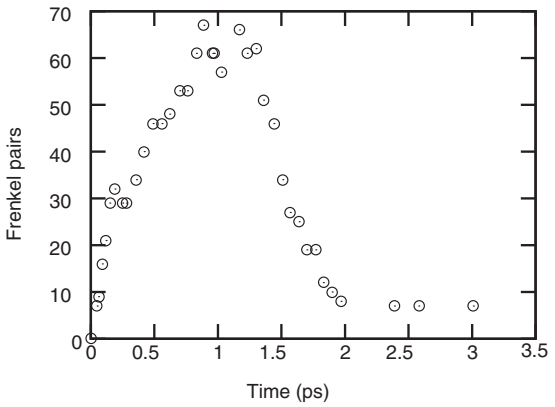

FIG. 3. Graph of the evolution of the number of "Frenkel pairs" in the system for a typical event. The definition of a "Frenkel pair" in the cascade phase is as follows: we define each site in the undamaged crystal as a reference point and then count the number of atoms in the final configuration within a sphere of half the neighbor distance of each reference point. The "Frenkel pair" count is the number of cells with two atoms in this range and no neighboring lattice site with zero associated atoms. Despite this arbitrariness, it is clear that the typical cascade lasts for approximately 2 ps.

thermal fluctuations was sometimes observed near the surface at 300 K. To quantify the damage, we counted the number of interstitials and adatoms, reporting "Frenkel pair" yields which include defects seen in clusters and craters. We also monitored how far individual atoms have moved. We note that a perfectly flat surface is not an ideal sink: the defect retains its identity as an adatom in a similar way to that predicted for perfect grain boundaries or inhomogeneous interfaces.[4,24] Thus there are no sinks in our simulation.

We gathered statistics over 90 runs, finding that apparent measured damage peaked at around 1 ps and was largely settled by 2–3 ps. Each run continued for a further 5 ps during which at most one pair recombined. The time dependence of the number of Frenkel pairs is shown in Fig. 3.

There was significant variation between different runs: a few collisions producing almost no visible damage, typically when the primary knock-on atom was channeled between lattice planes and the cascade was well below the surface. This implies that the surface itself has a role in the damage created, a conclusion supported by the correlation between penetration depth and damage (see Fig. 4 and further analysis in Supplemental Material[43]). Most of the defects end up on the surface, consistent with a stress wave[44] or an active attraction mechanism[4,45] rather than a sink for random-walking particles.

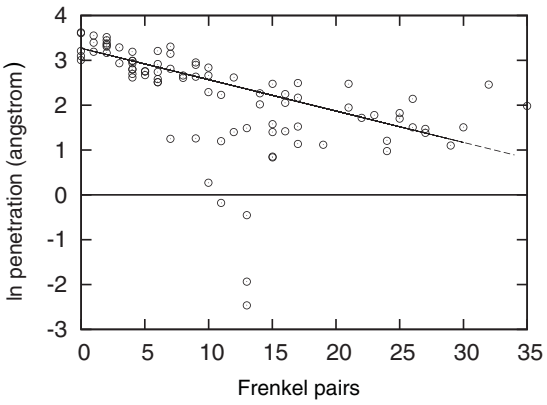

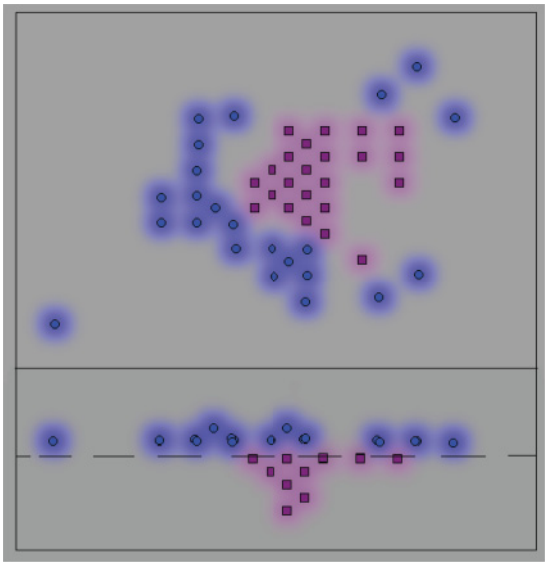

FIG. 4. (Color online) (a) Number of Frenkel defects (N_F) produced as a function of penetration depth (d), defined as the lowest point reached by the Ar ion below the average position of the surface layer. The anomalous very low values of d correspond to bouncing off the surface and are excluded from the fit line. $d = 23.3(2)\exp[-0.074(5)N_F]$ (b) Typical distribution of final defects, for a high-yield collision, 27 Frenkel pairs, viewed from above the (110) surface (top) and a perpendicular slice ($\bar{1}$10) (bottom); shown are vacancies (red squares) and interstitials (blue circles, with shaded halo). A background shading was added to highlight the six clusters of sizes 17, 2, 1, 1, 1, and 1. On average, 11.9(10) Frenkel pairs were formed per cascade, of which 10.3(8) produce adatoms, the other evaporating or (rarely) forming subsurface interstitials; 72(3)% of the vacancies formed were in the single crater; the others were predominantly subsurface. The Ar atom was ejected from the system 41(6)% of the time.

IV. DISCUSSION

Figure 2 appears to show spectacular agreement, but quantitative comparison with the experimental statistics is not straightforward. There will be a systematic bias toward including those events causing more damage. Events producing no damage are obviously not included in the experimental statistics, and isolated single adatoms cannot be reliably imaged in the STM. This means that some events will not be observed experimentally. To account for this we include in the MD statistics only those events which produce at least one adatom cluster with a three adatom size, in which case the calculated adatom yield rises to 16.2(9) with 12.6(8) visible (Fig. 2). It can be seen in Figs. 1 and 4 that the vacancies form a three-dimensional crater while the adatoms are in a halo of two-dimensional plates. Both the experiment and simulation (Figs. 1 and 4) observe the vacancies to be in a centralized circular cluster at the surface. The MD results show this vacancy cluster to be a cone, but our STM analysis assumes a depth of one monolayer. So the STM results in Fig. 2 are also a lower bound.

The adatom defects were observed to be distributed around the impact with a radius of 9.6(4) Å, in reasonable agreement with the calculated value of 8.7(3) Å or, ignoring simulations forming three or fewer Frenkel pairs, 9.4(3) Å.

An additional 30 simulations were performed for $30 \pm 5^\circ$ incidence. This had a notable effect on the distribution of the penetration depth, reducing the average depth to 6.6(9) Å. The Frenkel pair production increased to 17.7(12). These changes arise from a reduction in high penetration events (Fig. 4), which were enhanced by channeling in the case of 0° incidence. Another 30 simulations were conducted at 300 K to investigate temperature effects, the results of which closely match the 144-K results, in terms of yield and distribution [the mean penetration depth is slightly reduced to 8.7(12) Å]. This contrasts with STM images at 300 K which show a greatly decreased yield of adatoms, suggesting that surface recombination is important on the millisecond time scale at 300 K.

Figure 2 shows that the damage accumulates as midsized (3–10) clusters in the experiment, while the simulation shows more individual adatoms. This strongly implies that there is some short-ranged absorption of single adatoms into immobile clusters on a time scale longer than a few ps. To check, we used static relaxation and molecular dynamics (Arrhenius analysis of self-diffusion rates) to calculate barriers for adatom hopping on the (110) surface. The two methods give consistent, anisotropic, results: 0.32 eV [$1\bar{1}0$] and 1.17 eV [001]. Equating the attempt frequency to the Debye frequency gives a hop frequency on the second time scale at 144 K. Thus surface motion is highly significant at 300 K,[46] and even at 144 K there is enough time for single adatoms to coalesce and join larger clusters. Vacancy and larger adatom clusters are significantly less mobile, as in fcc Rh.[47] In Fig. 5 we give details of calculated migration barriers around and away from small surface clusters, which also shows a [$1\bar{1}0$] dimer bonding of 0.31 eV and much weaker binding across [001].

We have also monitored the distribution of local stress[35] around the impact site (see SM movies). This is the standard method for describing the formation of impact craters and provides an unconventional viewpoint for the radiation damage cascade process. The damage cascade at the surface has the structure of a stress wave propagating outward and then upward from the impact: defect clusters are created fully formed at the surface, vacancies from the initial impact and the halo of interstitials from the wave (see Fig. 6). Several other visualizations of this process for different types of cascade are given in SM. This is consistent with observations of sputtered cluster formation at much higher energies in Au[48,49] and with recent bulk simulations in iron.[7–9] In the SM, we identify five types of collision by tracing the displacement of the atoms from their initial positions. The majority are either high yield, when the cascade overlaps the surface and stress analysis shows that local stresses have wavelike structures as opposed to a classical disorganized "thermal spike," or low yield when the cascade occurs deeper in the sample and most defects recombine. However, some 30% are hybrids: double cascades, with distinct surface and deep events which do not exchange defects; surface cascades, which eject defects into the bulk or along the surface; and surface events, with

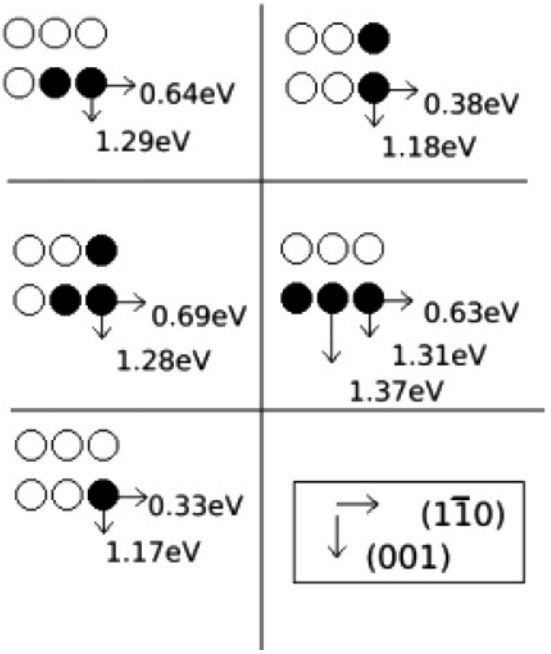

FIG. 5. Schematic showing surface diffusion barriers from static calculation for adatoms and small clusters on a (110) surface. [$1\bar{1}0$] is along the surface channels, [001] is across the channels. The barriers given are for the movement of a single adatom along the direction shown (not the whole cluster) until the saddle point is reached; the adatom is free to relax away or toward the surface.

secondary overlapping events. Curiously, not only does the subsurface damage heal but there is no evidence of liquid-like self-diffusion within the cascade; despite the apparent large creation of Frenkel defects in Fig. 3, most atoms return to their original sites.

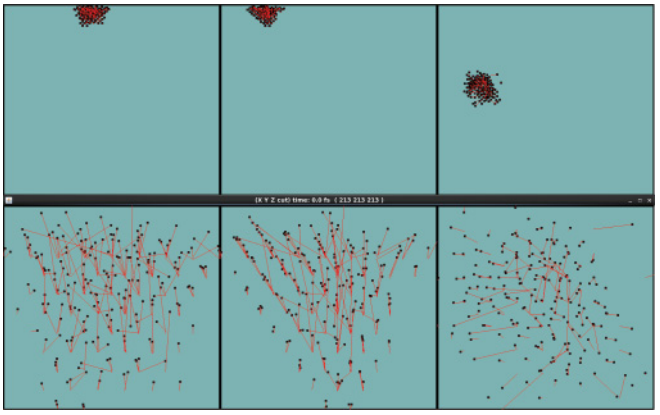

FIG. 6. (Color online) Figure showing the relationship between initial and final positions of atoms after a typical surface cascade. Black squares indicate atoms which have at least two near neighbors different from the initial state. Red lines link the initial position of atoms to their final position. Upper panel: x, y, and z projections for the whole system, showing the shape of the stress flow creating the crater. Lower panel: closeup of the upper panel, showing that the displacements have a systematic structure resulting from the crater-forming stress wave, rather than the disordered pattern one might expect from localized melting.

Another interesting feature is the one-dimensional focusing of the stress along close-packed directions. This mechanism is similar to a conventional collision-replacement sequence (CRS) for interstitial migration, but because it is energy that is being transmitted, the interstitial migration barrier is irrelevant. These focused stress waves can cause an interstitial to appear remotely when they encounter a lower barrier, e.g., at the surface (see SM). Sometimes no defect is produced, but these failed-CRS events provide a soliton mechanism for quickly removing heat from the cascade.

V. SUMMARY

We have imaged individual radiation damage events in Cu directly using STM and shown that the qualitative images are well reproduced by MD simulation. The observed cluster-size distribution is different in the experiment and simulation, an effect we believe to be due to adatom migration to larger clusters on the time scale of seconds. Quantitative defect yield counts show very good agreement between MD and the experiment.

ACKNOWLEDGMENTS

We thank G. E. Isted for assistance with experimental work, the Seventh Framework Programme GETMAT and PERFORM-60 collaborations for useful discussions, EPCC for central processing unit time, and the Engineering and Physical Sciences Research Council (EPSRC) Scottish Condensed Matter Doctoral Training Centre (CM-DTC) for a studentship (G.J.G.).

[1] M. J. Norgett, M. T. Robinson, and I. M. Torrens, Nucl. Eng. Des. **33**, 50 (1975).
[2] M. T. Robinson and I. M. Torrens, Phys. Rev. B **9**, 5008 (1974).
[3] Z. Yao, M. J. Caturla, and R. Schaublin, J. Nucl. Mater. **367**, 298 (2007).
[4] X-M. Bai, A. F. Voter, R. G. Hoagland, M. Nastasi, and B. P. Uberuaga, Science **327**, 1631 (2010).
[5] W. J. Phythian, R. E. Stoller, A. J. E. Foreman, A. F. Calder, and D. J. Bacon, J. Nucl. Mater. **223**, 245 (1995).
[6] D. J. Bacon, Y. N. Osetsky, R. Stoller, and R. E. Voskoboinikov, J. Nucl. Mater. **323**, 152 (2003).
[7] A. F. Calder, D. J. Bacon, A. V. Barashev, and Y. N. Osetsky, Philos. Mag. **90**, 863 (2010).
[8] A. F. Calder, D. J. Bacon, A. V. Barashev, and Y. N. Osetsky, Philos. Mag. Lett. **88**, 43 (2008).
[9] D. J. Hepburn and G. J. Ackland, Phys. Rev. B **78**, 165115 (2008).
[10] K. O. E. Henriksson, K. Nordlund, and J. Keinonen, Phys. Rev. B **76**, 245428 (2007).
[11] M. Samaras and P. M. Derlet, H. Van Swygenhoven, and M. Victoria, Phys. Rev. Lett. **88**, 125505 (2002).
[12] K. Nordlund and F. Gao, Appl. Phys. Lett. **74**, 2720 (1999).
[13] D. J. Bacon, F. Gao, and Y. N. Osetsky, J. Nucl. Mater. **276**, 1 (2000).
[14] M. J. Caturla, N. Soneda, E. Alonso, B. D. Wirth, T. Diaz de la Rubia, and J. M. Perlado, J. Nucl. Mater. **276**, 13 (2000).
[15] J. J. Blackstock and G. J. Ackland, Philos. Mag. A **81**, 2127 (2001).
[16] B. P. Uberuaga, R. G. Hoagland, A. F. Voter, and S. M. Valone, Phys. Rev. Lett. **99**, 135501 (2007).
[17] T. Kadoyoshi, H. Kaburaki, F. Shimizu, H. Kimizuka, S. Jitsukawa, and J. Li, Acta Mater. **55**, 3073 (2007).
[18] E. M. Bringa and R. E. Johnson, Phys. Rev. Lett. **88**, 165501 (2002).
[19] E. M. Bringa, R. E. Johnson, and M. Jakas, Phys. Rev. B **60**, 15107 (1999).
[20] Y. N. Osetsky, D. Rodney, and D. J. Bacon, Philos. Mag. **86**, 2295 (2006).
[21] C. A. English and M. L. Jenkins, Philos. Mag. **90**, 821 (2010).
[22] C. A. English, M. L. Jenkins, and B. L. Eyre, Nature (London) **263**, 400 (1978); Philos. Mag. **38**, 97 (1978).
[23] N. Nita, R. Schaublin, and M. Victoria, J. Nucl. Mater. **329–333**, 953 (2004).
[24] M. J. Demkowicz, R. G. Hoagland, and J. P. Hirth, Phys. Rev. Lett. **100**, 136102 (2008).
[25] B. D. Wirth, Science **318**, 923 (2007).
[26] K. Arakawa, Science **318**, 956 (2007).
[27] Y. Matsukawa and S. J. Zinkle, Science **318**, 959 (2007).
[28] S. J. Zinkle and K. Farrell, J. Nucl. Mater. **168**, 262 (1989).
[29] E. M. Bringa and R. E. Johnson, Astrophys. J. **603**, 159 (2004).
[30] E. M. Bringa, R. E. Johnson, and R. M. Papaleo, Phys. Rev. B **65**, 094113 (2002).
[31] P. Weightman, D. S. Martin, R. J. Cole, and T. Farrell, Rep. Prog. Phys. **68**, 1251 (2005).
[32] P. Hofmann, K. C. Rose, V. Fernandez, A. M. Bradshaw, and W. Richter, Phys. Rev. Lett. **75**, 2039 (1995).
[33] G. E. Isted, P. D. Lane, R. J. Cole, M. Caffio, and R. Schaub, Phys. Rev. B. **83**, 155403 (2011).
[34] G. Costantini, F. Buatierde Mongeot, C. Borango, and U. Valbusa, Phys. Rev. Lett. **86**, 838 (2001).
[35] G. J. Ackland *et al.*, Comp. Phys. Comm. **182**, 2587 (2011).
[36] G. J. Ackland, G. I. Tichy, V. Vitek, and M. W. Finnis, Philos. Mag. A **56**, 735 (1987).
[37] W. E. Wallace, and G. J. Ackland, Surf. Sci. Lett. **275**, L685 (1992).
[38] A. J. E. Foreman, W. J. Phythian, and C. A. English, Philos. Mag. A **66**, 671 (1992).
[39] J. F. Ziegler, J. P. Biersack, and U. Littmark, *The Stopping and Range of Ions in Solids* (Pergamon, New York, 1985).
[40] Equating the excess energy in a region to the heat flow through the region, the characteristic time scale of cooling can be found as $t = 3Nk/2KxD$, where D is the number of directions that heat may flow through the system and x is the length of the system, where it has been assumed the system is cubic and that k does not vary significantly over the temperature difference. For this system size, this calculation gives a thermal relaxation time of 0.16 ps.
[41] C. P. Race, D. R. Mason, M. W. Finnis, W. M. C. Foulkes, A. P. Horsfield, and A. P. Sutton, Rep. Prog. Phys. **73**, 116501 (2010).

[42]J. le Page, D. R. Mason, C. P. Race, and W. M. C. Foulkes, New J. Phys. **11**, 013004 (2009).
[43]See Supplemental Material at http://link.aps.org/supplemental/10.1103/PhysRevB.85.094111.
[44]I. S. Bitensky and E. S. Parilis, Nucl. Instrum. Methods **21**, 26 (1987).
[45]G. Ackland, Science **327**, 1587 (2010).
[46]P. D. Lane, G. E. Isted, and R. J. Cole, Phys. Rev. B **82**, 075416 (2010).
[47]G. L. Kellogg, Prog. Surf. Sci. **53**, 217 (1996).
[48]R. C. Birtcher and S. E. Donnelly, Nucl. Instrum Methods **148**, 194 (1999).
[49]L. E. Rehn, R. C. Birtcher, S. E. Donnelly, P. M. Baldo, and L. Funk, Phys. Rev. Lett. **87**, 207601 (2001).